On Feasible Region of Droop-based Fast Frequency Response Controller Parameters of Wind Turbines

Junkai Huang, *Student Member*, *IEEE* and Yan Xu, *Senior Member*, *IEEE*

***Abstract*—Droop-based fast frequency response (FFR) control of wind turbines can improve the frequency performance of power systems with high penetration of wind power. Explicitly formulating the feasible region of the droop-based FFR controller parameters can allow system operators to conveniently assess the feasibility of FFR controller parameter settings to comply with system frequency security, and efficiently tune and optimize FFR controller parameters to meet frequency security requirements. However, the feasible region of FFR controller parameters is inherently nonlinear and implicit because the power point tracking controllers of wind turbine would counteract the effect of FFR controllers. To address this issue, this letter proposes a linear feasible region formulation method, where frequency regulation characteristics of wind turbines, the dead band, and reserve limits of generators are all considered. The effectiveness of the proposed method and its application is demonstrated on a 10-machine power system.**

***Index Terms*—Wind turbine, fast frequency response, feasible region, frequency security.**

I. Introduction

WIND turbines can provide frequency support to a power system via fast frequency response (FFR) controllers [1]. The droop-based FFR controller allows a wind turbine to provide primary frequency regulation (PFR) support, which becomes an essential requirement in modern power systems [2].

In practice, frequency controllers of generators are supposed to be tuned to keep the steady-state frequency deviation of the system within an allowable range when there is a large power imbalance event [3]. In this letter, we define the parameter settings that satisfy the steady-state frequency deviation requirement of the system as the feasible region of controller parameters. To formulate the feasible region, the power-frequency (*P-f*) characteristic curve of a generator can be utilized since it can conveniently determine the steady-state frequency deviation of the system. For a synchronous generator, the *P-f* characteristic can be expressed as a piecewise linear function that is determined by the droop coefficient, the dead band, and the reserve limit [4]. However, the existing research works show that the *P-f* characteristic of a wind turbine with an FFR controller is nonlinearly and implicitly related to the FFR controller parameter because of the involvement of the power point tracking controller of wind turbine [5]. Therefore, formulating the feasible region of FFR controller parameters of wind turbine is difficult. In the existing literature, an accurate feasible region can be formulated through the exhaustive searching method, which is time-consuming. Alternatively, a linearized feasible region can be obtained by utilizing transfer function modeling [6]; however, the linearization error could be significant.

This letter aims to find a trade-off between calculation efficiency and approximation accuracy so that power system operators can conveniently assess whether FFR controller parameter settings can comply with frequency security. FFR parameters can be efficiently tuned and optimized to meet the frequency security requirement. To this end, a method is proposed for formulating the linear feasible region of FFR controller parameters of wind turbine, where the frequency regulation characteristics of wind turbines, the dead band, and the reserve limit of generators are all considered.

II. Feasible Region of Droop-based FFR Controller Parameters of Wind Turbine

The typical frequency response of a power system following a power imbalance event is presented in Fig. 1. The frequency security can be assessed according to the maximum frequency deviation and the steady-state frequency deviation. In this letter, the FFR controller parameter settings for steady-state frequency security are studied. As specified in the transmission code, the steady-state frequency deviation should not exceed a certain threshold. For example, the permissible steady-state frequency deviation for the Continental Europe Synchronous Area is 0.2 Hz, and that in the Nordic Area is 0.5 Hz [7]. The feasible region of FFR controller parameters is composed of all the FFR controller parameter settings that satisfy the steady-state frequency deviation requirement of the system.

Manuscript received: June 8, 2023; revised: September 4, 2023; accepted: November 20, 2023. Date of CrossCheck: November 20, 2023. Date of online publication: January 2, 2024.

The work was supported in part by Ministry of Education (MOE), Republic of Singapore (No. AcRF TIER-1 RT11/22).

J. Huang and Y. Xu (corresponding author) are with School of Electrical and Electronic Engineering, Nanyang Technological University, 50 Nanyang Avenue, Singapore (e-mail: junkai001@e.ntu.edu.sg; xuyan@ntu.edu.sg).

DOI: 10.35833/MPCE.2023.000394

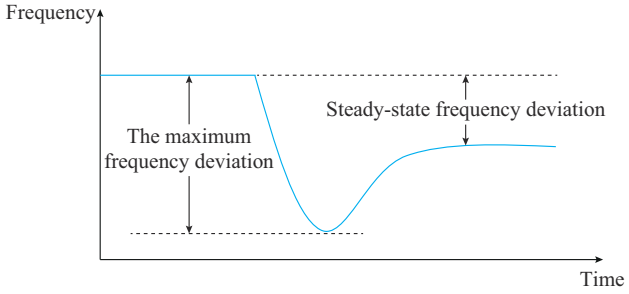

Fig. 1. Illustration of typical frequency response of a power system following a power imbalance event.

The nonlinear feasible region is derived in this section. Without loss of generality, the feasible region derived below is for the frequency drop case, but it can be similarly derived for the frequency rise case. Denoting $\Delta f_{\rm ss}^{\rm lower}$ and $\Delta f_{\rm ss}^{\rm upper}$ as lower and upper limits of the steady-state frequency deviation $\Delta f_{\rm ss}$, respectively, both of which are negative, and the constraint is written as:

$$\Delta f_{\rm ss}^{\rm lower} \le \Delta f_{\rm ss} \le \Delta f_{\rm ss}^{\rm upper} \tag{1}$$

To obtain the feasible region of FFR parameters, $\Delta f_{\rm ss}$ should be expressed as a function of FFR parameters. $\Delta f_{\rm ss}$ can be determined by using the *P-f* characteristics of each generator. Denoting the power deficit as ΔL, the steady-state frequency deviation occurs when the sum of incremental power of each generator equals ΔL:

$$\sum_{j=1}^{N_{\rm wind}} \Delta P_{{\rm ffr},j} + \sum_{i=1}^{N_{\rm gen}} z_i\left(\Delta f_{\rm ss}\right) + \sum_{k=1}^{N_{\rm load}} z_k\left(\Delta f_{\rm ss}\right) = \Delta L \tag{2}$$

where $N_{\rm wind}$, $N_{\rm gen}$, and $N_{\rm load}$ are the numbers of wind turbines, synchronous generators, and load, respectively; $\Delta P_{{\rm ffr},j}$ is the incremental power of the $j^{\rm th}$ wind turbine; $z_i(\cdot)$ is the *P-f* characteristic of the $i^{\rm th}$ generator, denoting a piecewise linear function for the determined droop coefficient, dead band, and reserve limit; and $z_k(\cdot)$ is the damping effect of the $k^{\rm th}$ load. As illustrated in [8], the mathematical form of load damping $z_k(\cdot)$ is similar to that of $z_i(\cdot)$, and thus $z_k(\cdot)$ will be ignored for simplifying derivation.

The block diagram of the wind turbine with a droop-based FFR controller is given in Fig. 2, where an overspeed deloading method is considered in this letter for power point tracking.

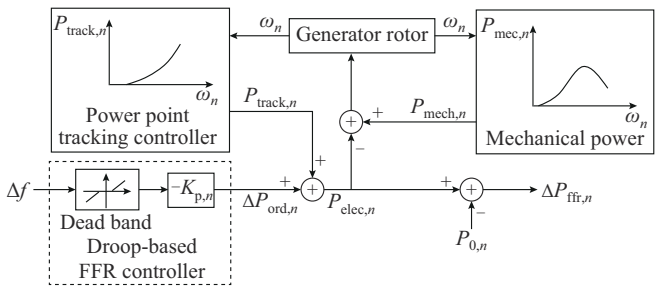

Fig. 2. Block diagram of wind turbine with a droop-based FFR controller.

For the $n^{\rm th}$ wind turbine, the command from the power point tracking controller $P_{{\rm track},n}$ is represented as:

$$P_{{\rm track},n} = k_{{\rm dl},n}\omega_n^3 \tag{3}$$

where $k_{{\rm dl},n}$ is the deloading curve coefficient, which depends on a given initial operating point; and ω_n is the rotor speed.

The command from the FFR controller $\Delta P_{{\rm ord},n}$ can be written as:

$$\Delta P_{{\rm ord},n} = -K_{{\rm p},n}\left(\Delta f_{\rm ss} - db_n\right) \tag{4}$$

where $K_{{\rm p},n}$ is the FFR parameter; and db_n is the regulation dead band value, which is negative if $\Delta f_{\rm ss} < 0$, and positive if $\Delta f_{\rm ss} > 0$.

Thus, the power output of the wind turbine $P_{{\rm elec},n}$ should be:

$$P_{{\rm elec},n} = P_{{\rm track},n} + \Delta P_{{\rm ord},n} = k_{{\rm dl},n}\omega_n^3 - K_{{\rm p},n}\left(\Delta f_{\rm ss} - db_n\right) \tag{5}$$

At the steady state, the mechanical power of the wind turbine $P_{{\rm mech},n}$ should equal $P_{{\rm elec},n}$, i.e.:

$$P_{{\rm mech},n} = P_{{\rm elec},n} = P_{{\rm track},n} + \Delta P_{{\rm ord},n} \tag{6}$$

According to [6], for a given wind speed, the mechanical power $P_{{\rm mech},n}$ can be written as a nonlinear function of rotor speed (7), where the pitch angle is considered to be zero when using the overspeed deloading method.

$$P_{{\rm mech},n} = 0.5\rho A_{\rm r} v_{\rm w}^3 C_{\rm p}\left(\omega_n\right) \tag{7}$$

where ρ is the air density; $A_{\rm r}$ is the area swept by the rotor blades; $v_{\rm w}$ is the wind speed; and $C_{\rm p}$ is the power coefficient, which would be a function of ω_n if wind speed and pitch angle are given.

Approximations are used to reveal the nonlinear feature of feasible region of FFR controller parameter in the following content. By using second-order polynomials to approximate the mechanical power, as indicated in [9], and applying the second-order Taylor expansion to the signal from power point tracking, $P_{{\rm mech},n}$ and $P_{{\rm track},n}$ can be represented as:

$$P_{{\rm mech},n} = m_{2,n}\omega_n^2 + m_{1,n}\omega_n + m_{0,n} \tag{8}$$

where $m_{2,n}$, $m_{1,n}$, and $m_{0,n}$ are constants.

$$P_{{\rm track},n} = 3k_{{\rm dl},n}\omega_{0,n}\omega_n^2 - 3k_{{\rm dl},n}\omega_{0,n}^2\omega_n + k_{{\rm dl},n}\omega_{0,n}^3 \tag{9}$$

where $\omega_{0,n}$ is the initial rotor speed of the $n^{\rm th}$ wind turbine.

According to the derivation process in [5], the steady-state incremental power of a wind turbine can be derived as:

$$\begin{cases} \Delta P_{{\rm ffr},n} = g_n\left(K_{{\rm p},n}, \Delta f_{\rm ss}\right) = P_{{\rm track},n} + \Delta P_{{\rm ord},n} - P_{0,n} = \\ \quad \left(\dfrac{k_{1,n}m_{2,n}}{2k_{2,n}^2} - \dfrac{m_{1,n}}{2k_{2,n}}\right)\sqrt{k_{1,n}^2 - 4k_{2,n}\left[k_{0,n} + K_{{\rm p},n}\left(\Delta f_{\rm ss} - db_n\right)\right]} - \\ \quad \dfrac{m_{2,n}}{k_{2,n}}K_{{\rm p},n}\left(\Delta f_{\rm ss} - db_n\right) + \left(\dfrac{k_{1,n}^2 m_{2,n}}{2k_{2,n}^2} - \dfrac{k_{0,n}m_{2,n}}{k_{2,n}} - \right. \\ \quad \left. \dfrac{k_{1,n}m_{1,n}}{2k_{2,n}} + m_{0,n}\right) - P_{0,n} \\ k_{0,n} = m_{0,n} - k_{{\rm dl},n}\omega_{0,n}^3 \\ k_{1,n} = m_{1,n} + 3k_{{\rm dl},n}\omega_{0,n}^2 \\ k_{2,n} = m_{2,n} - 3k_{dl,n}\omega_{0,n} \end{cases} \tag{10}$$

where g_n is the function representing the relationship among $\Delta P_{{\rm ffr},n}$, $K_{{\rm p},n}$, and $\Delta f_{\rm ss}$; and $P_{0,n}$ is the initial power output of the wind turbine.

By substituting (10) into (2), the relationship between the

FFR controller parameters and Δf_{ss} can be obtained; however, Δf_{ss} cannot be explicitly expressed as a function of FFR controller parameters. Meanwhile, when system frequency drops, power support from each wind turbine cannot exceed its reserve, considering the wind turbine stability indicated in [10]. Thus, the following constraints are enforced:

$$0 \le g_n\left(K_{p,n}, \Delta f_{ss}\right) \le \Delta \bar{P}_{ffr,n} \quad n = 1, 2, ..., N_{wind} \tag{11}$$

where $\Delta \bar{P}_{ffr,n}$ is the reserve of the n^{th} wind turbine.

To summarize, the feasible region of FFR controller parameters is jointly determined by (1), (2), (10), and (11). Note that the relationship described by (10) can also be obtained by using (3) and (7) without approximation when formulating the feasible region.

III. Linearization of Feasible Region of Droop-based FFR Controller Parameter

As indicated in Section II, the feasible region of droop-based FFR controller parameters is nonlinear and implicit, which can be considered as a mapping from the feasible region of ΔP_{ffr} (i.e., incremental power of wind turbines), and can be written as:

$$\Delta L - \sum_{i=1}^{N_{gen}} z_i\left(\Delta f_{ss}^{lower}\right) \le \sum_{j=1}^{N_{wind}} \Delta P_{ffr,j} \le \Delta L - \sum_{i=1}^{N_{gen}} z_i\left(\Delta f_{ss}^{upper}\right) \tag{12}$$

$$0 \le \Delta P_{ffr,n} \le \Delta \bar{P}_{ffr,n} \quad n = 1, 2, ..., N_{wind} \tag{13}$$

The constraint (12) represents two hyperplanes whose domain is defined by (13). Therefore, the hyperplane can be written in a general form:

$$\sum_{j=1}^{N_{wind}} \Delta P_{ffr,j} - \Delta P_{req} = 0 \tag{14}$$

where ΔP_{req} is the power requirement from wind turbines.

The hyperplane (14) should be a facet of a N_{wind}-dimensional polytope whose vertices are intersections among (13) and (14). If there are M vertices, the vertex set is denoted as $\boldsymbol{P} = \left[\Delta \boldsymbol{P}_{ffr}^{(1)}, \Delta \boldsymbol{P}_{ffr}^{(2)}, \ldots, \Delta \boldsymbol{P}_{ffr}^{(M)}\right]^T$, where $\Delta \boldsymbol{P}_{ffr}^{(o)} = \left[\Delta P_{ffr,1}^{(o)}, \Delta P_{ffr,2}^{(o)}, \ldots, \Delta P_{ffr,n}^{(o)}\right]^T$ represents the o^{th} vertex. $\boldsymbol{P}^{lower}$ and $\boldsymbol{P}^{upper}$ denote vertex sets for Δf_{ss}^{lower} and Δf_{ss}^{upper}, respectively.

Since Δf_{ss} is given, $\Delta P_{ffr,n}$ is a nonlinear function of $K_{p,n}$, i.e., $\Delta P_{ffr,n} = g_n\left(K_{p,n}\right)$. Thus, the hyperplane (14) of ΔP_{ffr} can be mapped to a hypersurface of K_p, i.e.:

$$\sum_{j=1}^{N_{wind}} g_j\left(K_{p,j}\right) - \Delta P_{req} = 0 \tag{15}$$

The domain of (15) is determined by:

$$0 \le g_n\left(K_{p,n}\right) \le \Delta \bar{P}_{ffr,n} \quad n = 1, 2, ..., N_{wind} \tag{16}$$

Then, the hypersurface (15) should be a surface with the vertices that are intersections among (15) and (16). The corresponding vertex set is denoted as $\boldsymbol{K} = [\boldsymbol{K}_p^{(1)}, \boldsymbol{K}_p^{(2)}, \ldots, \boldsymbol{K}_p^{(M)}]^T$, where $\boldsymbol{K}_p^{(o)} = [\boldsymbol{K}_{p,1}^{(o)}, \boldsymbol{K}_{p,2}^{(o)}, \ldots, \boldsymbol{K}_{p,n}^{(o)}]^T$ represents the o^{th} vertex. $\boldsymbol{K}$ is nonlinearly mapped from $\boldsymbol{P}$ for a given Δf_{ss}. $\boldsymbol{K}^{lower}$ and $\boldsymbol{K}^{upper}$ denote the vertex sets mapped from $\boldsymbol{P}^{lower}$ and $\boldsymbol{P}^{upper}$, respectively.

For illustration, Fig. 3 shows an case of two wind turbines. The feasible region of ΔP_{ffr} should be a line segment with endpoints A and B, as shown in Fig. 3(a). The corresponding feasible region of K_p will be a curve segment with endpoints A′ and B′, and A′ and B′ are mapped from A and B (curve A′B′).

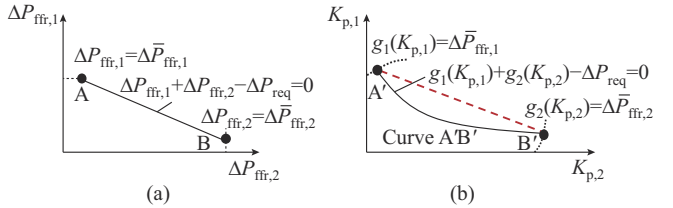

Fig. 3. Case of two wind turbines. (a) Hyperplane of feasible region of ΔP_{ffr}. (b) Hypersurface of feasible region of K_p and its approximation.

In Fig. 3 (b), curve A′B′ represents the FFR controller parameter settings that meet the frequency deviation lower limit. Therefore, to find an approximation that will not violate the frequency deviation, a linear boundary can be obtained by connecting A′ and B′ (the red dashed line in Fig. 3 (b)) on condition that $K_{p,1}$ is a decreasing convex function of $K_{p,2}$, i.e., $\partial K_{p,1}/\partial K_{p,2} < 0$ and $\partial^2 K_{p,1}/\partial K_{p,2}^2 > 0$.

The above condition can be further extended to multi-dimensional scenarios. In multi-dimensional space, the facet of a N_{wind}-dimensional polytope can be used as an approximation of the original feasible region of K_p if $K_{p,n}$ on the hypersurface (15) is a decreasing convex function of another parameter $K_{p,m}$, i. e., $\partial K_{p,n}/\partial K_{p,m} < 0$ and $\partial^2 K_{p,n}/\partial K_{p,m}^2 > 0$. $\partial K_{p,n}/\partial K_{p,m} < 0$ can be proven conveniently based on (15), and the proof of $\partial^2 K_{p,n}/\partial K_{p,m}^2 > 0$ is presented below.

Proof: based on (15), for the n^{th} wind turbine, it can be derived that:

$$K_{p,n} = g_n^{-1}\left(\Delta P_{req} - \sum_{j=1, j\ne n}^{N_{wind}} g_j\left(K_{p,j}\right)\right) \tag{17}$$

It can be proven that $\Delta P_{ffr,n} = g_n\left(K_{p,n}\right)$ is an increasing concave function according to its first-order and second-order derivatives. Because $\Delta P_{ffr,n} = g_n\left(K_{p,n}\right)$ is concave, $-\Delta P_{ffr,n} = -g_n\left(K_{p,n}\right)$ is convex, and thus, the sum $\left(\text{i.e., } -\sum g_j\left(K_{p,j}\right)\right)$ is convex, indicating that $\Delta P_{req} - \sum g_j\left(K_{p,j}\right)$ is convex. As indicated by Proposition 2 in [11], the inverse function $K_{p,n} = g_n^{-1}\left(\Delta P_{ffr,n}\right)$ is increasing and convex. Based on the composition rule, if h is a nondecreasing convex function and g is a convex function, the composition function $f = h \circ g$ is convex [12], where h refers to $g_n^{-1}\left(\Delta P_{ffr,n}\right)$, and g refers to $\Delta P_{req} - \sum g_j\left(K_{p,j}\right)$. Therefore, it can be proven that (17) is a convex function. According to [12], $\partial^2 K_{p,n}/\partial K_{p,m}^2 > 0$ since $K_{p,n}$ is a convex function of $K_{p,m}$.

The feasible region of droop-based FFR controller parameters includes two boundaries.

1) Boundary I

The Boundary I applies to all FFR parameters to meet the steady-state frequency security. Boundary I can be obtained by applying the linear regression method to vector $\boldsymbol{K}$. The

vector $\boldsymbol{K}$ can be calculated according to the vector $\boldsymbol{P}$ that satisfies (13) and (14). The obtained hyperplanes can be represented as:

$$\begin{cases} \sum_{j=1}^{N_{\text{wind}}} c_j^{\text{lower}} K_{\text{p},j} - c_0^{\text{lower}} \geq 0 \\ \sum_{j=1}^{N_{\text{wind}}} c_j^{\text{upper}} K_{\text{p},j} - c_0^{\text{upper}} \leq 0 \end{cases} \tag{18}$$

where the superscripts lower and upper represent that the regression coefficient c is for the lower limit $\Delta f_{\text{ss}}^{\text{lower}}$ and the upper limit $\Delta f_{\text{ss}}^{\text{upper}}$, respectively. Note that the second constraint in (18) may cause the FFR controller parameters to violate $\Delta f_{\text{ss}}^{\text{upper}}$ slightly. However, this is acceptable because a larger $\Delta f_{\text{ss}}^{\text{upper}}$ indicates a more secure frequency deviation.

2) Boundary II

The Boundary II applies to K_{p} of an individual wind turbine to determine its upper and lower bounds. For the n^{th} wind turbines, the lower limit for $K_{\text{p},n}$ will be the minimum value of the n^{th} column of $\boldsymbol{K}^{\text{lower}}$, which can be represented as:

$$K_{\text{p},n} \geq K_{\text{p},n}^{\text{lower}} = \max\left\{\min\left(\boldsymbol{K}_{i,n}^{\text{lower}} \middle| i = 1, 2, ..., M\right), 0\right\} \tag{19}$$

where $\boldsymbol{K}_{i,n}^{\text{lower}}$ is the i^{th} row and the n^{th} column element.

Similarly, the upper limit for $K_{\text{p},n}$ will be:

$$K_{\text{p},n} \leq K_{\text{p},n}^{\text{upper}} = \max\left\{\max\left(\boldsymbol{K}_{i,n}^{\text{lower}} \middle| i = 1, 2, ..., M\right), K_{\text{p0},n}\right\} \tag{20}$$

where $K_{\text{p0},n}$ is the $K_{\text{p},n}$ mapped from $\Delta \boldsymbol{P}_{\text{ffr}} = \left[0, 0, \ldots, \Delta \bar{P}_{\text{ffr},n}, \ldots, 0, 0\right]^{\text{T}}$.

IV. Case Studies

The proposed feasible region can be applied for fast feasibility assessment of FFR controller parameter settings and its optimization for frequency control. Case studies are conducted on a power system with 10 synchronous machines whose parameters are obtained from the New England test system. Considering a generator outage of 800 MW capacity, the post-fault nonlinear *P-f* characteristic is represented by the blue curve, as shown in Fig. 4. The increased power of generators should equal power deficit of 800 MW at the steady state, and thus the frequency deviation should be –0.304 Hz according to Fig. 4.

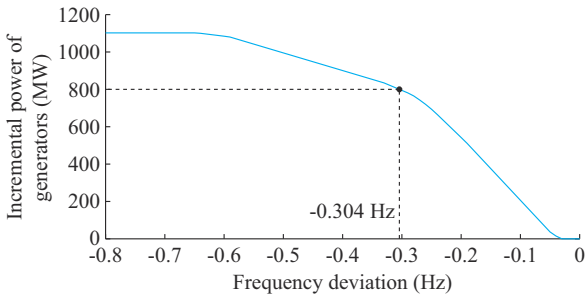

Fig. 4. *P-f* characteristics after a generator outage of 800 MW capacity.

A. Verification of Accuracy and Calculation Efficiency

The proposed method is compared with the exhaustive searching method that serves the benchmark and the traditional method that forms a linear feasible region based on transfer function models.

Firstly, two wind farms are added to the system, and their parameters are given in Table I. The two wind farms are modeled as two equivalent wind turbines. $\Delta f_{\text{ss}}^{\text{upper}}$ is set to be –0.250 Hz, and $\Delta f_{\text{ss}}^{\text{lower}}$ is increased from –0.293 Hz to –0.260 Hz by a step size of 0.011 Hz. The feasible regions of FFR controller parameter are shown in Fig. 5.

TABLE I
Parameter of Wind Farms

Wind farm No.	Nominal power (MW)	Regulation-up reserve (MW)	Wind speed (m/s)	Dead band (Hz)
1	1000	51	9	±0.03
2	1200	57	8	±0.05

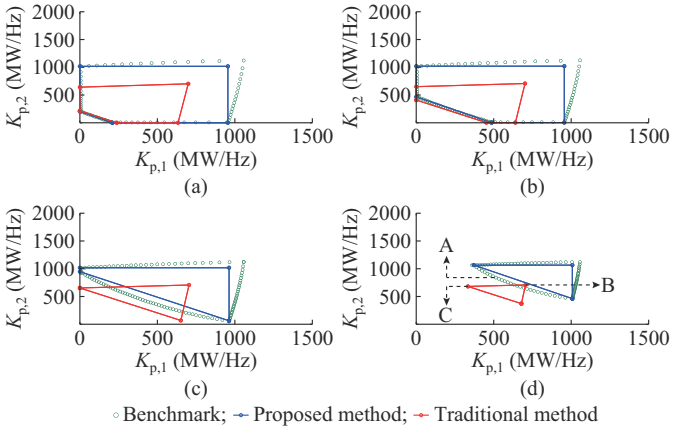

Fig. 5. Feasible region of FFR controller parameter when $\Delta f_{\text{ss}}^{\text{upper}} = -0.250$ Hz. (a) $\Delta f_{\text{ss}}^{\text{lower}} = -0.293$ Hz. (b) $\Delta f_{\text{ss}}^{\text{lower}} = -0.282$ Hz. (c) $\Delta f_{\text{ss}}^{\text{lower}} = -0.271$ Hz. (d) $\Delta f_{\text{ss}}^{\text{lower}} = -0.260$ Hz.

In Fig. 5(a) and (b), it can be observed that both the traditional method (red polygon) and the proposed method (blue polygon) can obtain feasible regions to approximate the benchmark. However, the blue polygon is much larger than the red polygon, indicating that the proposed method can obtain a more accurate feasible region. For example, the area of the blue polygon covers 89.42% of the area of the benchmark. However, as shown in Fig. 5(c), there is only a small part of the red polygon that is within the benchmark, while the blue region can still approximate the benchmark effectively. In Fig. 5(d), for the traditional method, the red polygon is almost all outside of the benchmark, indicating that the accuracy is about zero. However, as indicated by the blue polygon, the accuracy of the proposed method could reach 69.50%.

Dynamic simulation is carried out to validate the proposed method by using the system frequency response model illustrated in [1]. Three points at the boundaries are considered, i.e., points A-C in Fig. 5(d). According to the frequency deviation dynamics shown in Fig. 6, the dashed curve for A will exactly stabilize at $\Delta f_{\text{ss}}^{\text{lower}}$. As for the proposed method, because it is a conservative approximation, the absolute steady-state frequency deviation would be less than the ex-

pected value. However, the traditional method cannot meet the required Δf_{ss}^{lower} in this case.

Based on the simulation result, the error that occurs in the traditional method is explained by Fig. 7, which depicts the mechanical power captured by wind farm 2 from wind, power-rotor speed output trajectory, and the linearized mechanical power. When formulating the feasible region, the traditional method will use the linearized mechanical power to approximate the actual one. It can be found that the linearization error increases as the steady-state incremental active power from wind farm 2 increases. Similarly, errors will also be produced by the linearization of deloading curves.

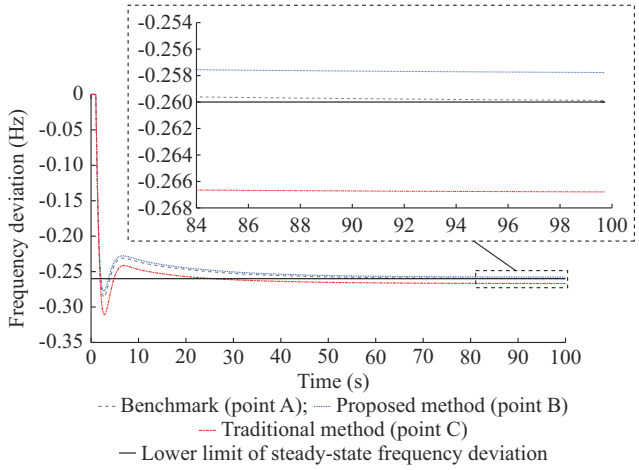

Fig. 6. Frequency deviation dynamics.

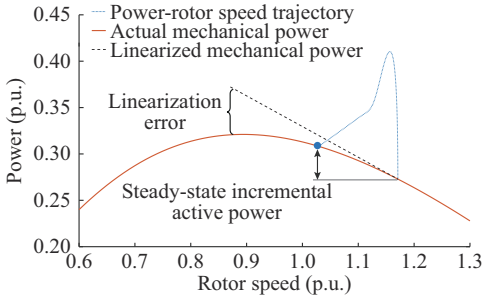

Fig. 7. Illustration for errors of traditional method.

Therefore, if Δf_{ss}^{lower} increases, more active power from wind turbines is required, and thus wind turbines will further deviate from initial points, thereby increasing the linearization error.

Then, the effectiveness of the proposed method as the wind farm number increases is investigated. Wind farms are represented as equivalent wind turbines for illustration in the following part. The uniform sampling method is used to reduce the computation burden. N_{sample} samples that satisfy the actual constraints are generated. N_{pro} and N_{tra} are defined as the numbers of samples that are within the feasible region given by the proposed method and traditional method, respectively. Therefore, the accuracy of the traditional method and the proposed method can be measured by N_{tra}/N_{sample} and N_{pro}/N_{sample}, respectively. The impacts are shown in Fig. 8, where the accuracies of both the proposed method and the traditional method decrease as the number of equivalent wind turbines increases, which is unavoidable if the nonlinear feasible region is linearized when the nonlinearity increases. Nevertheless, the accuracy of the proposed method is more than twice the accuracy of the traditional method.

Additionally, the calculation efficiency of the proposed method is compared with the exhaustive searching method. As shown in Table II, the calculation time of using the exhaustive equivalent wind turbines increases. In comparison, the calculation time of the proposed method could be much less. For example, to obtain the feasible region of 300 equivalent wind turbines, the exhaustive searching method takes more than 1 hour, while the proposed method costs 4.479 s only.

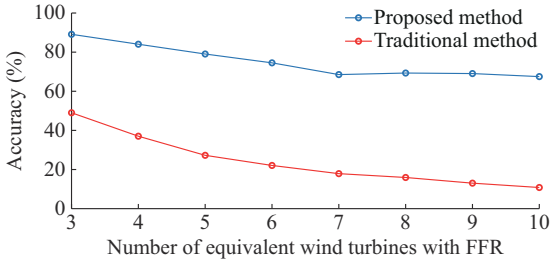

Fig. 8. Impacts of number of equivalent wind turbines on accuracy.

B. Application for Parameter Optimization

TABLE II
CALCULATION TIME COMPARISON

Number of equivalent wind turbines	Calculation time (s)	
	Exhaustive searching method	Proposed method
3	0.066	0.024
4	0.223	0.019
5	2.105	0.022
6	93.380	0.023
300	>3600.000	4.479

In this subsection, 300 equivalent wind turbines are considered for parameter optimization. The objective is to minimize the total power output of wind turbines after the above-mentioned power disturbance. The linear constraints are formed by the proposed method. For comparison, the original nonlinear and implicit constraints are used, and the optimization problem is solved by the method proposed in [5]. The calculation time is 238.46 s, and the objective function value is 25.70. For the proposed method, the optimization problem can be solved much more efficiently. The calculation time is reduced to 34.26 s, and the objective function value is 22.65, showing a significant improvement in both solution speed and solution quality as 85.63% and 11.86%, respectively.

V. CONCLUSION

This letter proposes a linearization method for obtaining the droop-based feasible region of FFR controller parameters, considering wind turbine characteristics, the dead band, and the reserve limit. Simulation results show that the feasi-

ble region can support fast and accurate feasibility assessment of FFR controller parameter settings and efficient optimization for frequency control. In the future, the proposed method can be used in frequency security-constrained power system optimization such as operational dispatch and real-time parameter tuning.

REFERENCES

[1] S. Wang and K. Tomsovic, "Fast frequency support from wind turbine generators with auxiliary dynamic demand control," *IEEE Transactions on Power Systems*, vol. 34, no. 5, pp. 3340-3348, Sept. 2019.

[2] X. Bao and L. Zhang, "Review of grid codes and implementation for wind farm frequency regulation," in *Proceedings of 2022 7th International Conference on Energy Science and Applied Technology (ESAT 2022)*, Yichang, China, May 2022, pp. 1-8.

[3] J. I. Yoo, Y. Kang, E. Muljadi *et al*., "Frequency stability support of a DFIG to improve the settling frequency," *IEEE Access*, vol. 8, pp. 22473-22482, Jan. 2020.

[4] P. Codani, Y. Perez, and M. Petit, *Electric Vehicles as a Mobile Storage Device*. Chichester: John Wiley & Sons, 2015.

[5] J. Huang, Z. Yang, J. Yu *et al*, "Optimization for DFIG fast frequency response with small-signal stability constraint," *IEEE Transactions on Energy Conversion*, vol. 36, no. 3, pp. 2452-2462, Sept. 2021.

[6] J. Dai, Y. Tang, Q. Wang *et al*., "Aggregation frequency response modeling for wind power plants with primary frequency regulation service," *IEEE Access*, vol. 7, pp. 108561-108570, Aug. 2019.

[7] H. Kuisti, M. Lahtinen, M. Nilsson *et al*. (2015, Apr.). NAG-frequency quality report. [Online]. Available: https://www. entsoe. eu/Documents/Publications/SOC/Nordic/2018/Frequency-quality.zip.

[8] P. Kundur, *Power System Stability and Control*. New York: McGraw-Hill, 1994.

[9] G. Zhang, F. Zhang, L. Ding *et al*., "Wind farm level coordination for optimal inertial control with a second-order cone predictive model," *IEEE Transactions on Sustainable Energy*, vol. 12, no. 4, pp. 2353-2366, Oct. 2021.

[10] L. Huang, H. Xin, L. Zhang *et al*. "Synchronization and frequency regulation of DFIG-based wind turbine generators with synchronized control," *IEEE Transactions on Energy Conversion*, vol. 32, no. 3, pp. 1251-1262, Sept. 2017.

[11] M. Mršević, "Convexity of the inverse function," *Teaching of Mathematics*, vol. 11, no.1, pp. 21-24, Jan. 2008.

[12] S. Boyd and L. Vandenberghe, *Convex Optimization*. Cambridge: Cambridge University Press, 2004.

Junkai Huang received the B.E. degree in automation and the M.E. degree in electrical engineering from Chongqing University, Chongqing, China, in 2018 and 2021, respectively. He is currently pursuing the Ph.D. degree in electrical engineering at Nanyang Technological University, Singapore. His research interests include control and optimization of renewable energy sources, and power system analysis.

Yan Xu received the B.E. and M. E degrees from South China University of Technology, Guangzhou, China, in 2008 and 2011, respectively, and the Ph.D. degree from The University of Newcastle, Newcastle, Australia, in 2013. He conducted postdoctoral research with the University of Sydney Postdoctoral Fellowship, Sydney, Australia, and then joined Nanyang Technological University (NTU), Singapore, with The Nanyang Assistant Professorship. He is now an Associate Professor at School of Electrical and Electronic Engineering and a Cluster Director at Energy Research Institute @ NTU (ERI@N), Singapore. He is serving as the Chairman for IEEE Power & Energy Society Singapore Chapter. His research interests include power system stability and control, microgrid, and data analytics for smart grid applications.